ADVANCED HEALTHCARE MATERIALS
www.advhealthmat.de

Synergistic Antitumor Effects of Doxorubicin-Loaded Carboxymethyl Cellulose Nanoparticle in Combination with Endostar for Effective Treatment of Non-Small-Cell Lung Cancer

*Mingqiang Li, Zhaohui Tang, Jian Lin, Yu Zhang, Shixian Lv, Wantong Song, Yubin Huang, and Xuesi Chen**

The multi-modal combination therapy is proved powerful and successful to enhance the antitumor efficacy in clinics as compared with single therapy modes. In this study, the potential of combining chemotherapy with antiangiogenic therapy for the treatment of non-small-cell lung cancer is explored. Towards this aim, OEGylated carboxymethyl cellulose–(2-(2-(2-methoxyethoxy)ethoxy)methyl)oxirane (CMC–ME_2MO) is prepared by treating CMC with ME_2MO in the alkaline aqueous solution, and used to efficiently carry doxorubicin (DOX) with high drug-loading content (16.64%) and encapsulation efficiency (99.78%). As compared to free DOX, the resulting nanoparticles show not only the favorable stability in vitro but also the prolonged blood circulation, improved safety and tolerability, optimized biodistribution, reduced systemic toxicity, and enhanced antitumor efficacy in vivo, indicates a potential utility in cancer chemotherapy. Furthermore, the combination of the DOX-loaded polysaccharide nanoparticles and antiangiogenic drug endostar provides synergistic effects of chemotherapy and antiangiogenic therapy, which shows the highest efficiency in tumor suppression. The combination approach of the DOX-containing nanomedicine and endostar for efficient treatment of non-small-cell lung cancer is first proposed to demonstrate the synergistic therapeutic effect. This synergistic combination proves to be a promising therapeutic regimen in cancer therapy and holds great potential for clinical application.

1. Introduction

The use of multiple drugs, known as combination therapy, has been widely used in the clinic and achieved immense popularity in cancer treatment.[1a] Among these, antiangiogenic drugs in combination with chemotherapeutic drugs are widely used as frontline therapy for the treatment of various human cancers.[2] As is known, both angiogenesis and cancer cell proliferation are the main features of tumor tissues.[3a] To progress and satisfy the proliferating tumor cells, tumors and the adjacent tissues are highly vascularized to supply nutrients and oxygen leading to tumor growth (angiogenesis).[4] Therefore, antiangiogenic therapy is an elegant modality in cancer treatment that aims to prevent the formation of the tumor blood vessels, resulting in the inhibition of tumor growth.[5a] On the other hand, vascular endothelial growth factor (VEGF), which is overexpressed and secreted mostly by tumor cells, can efficiently stimulate proliferation of endothelial cells and cause angiogenesis in tumor tissue.[6a] Thus, chemotherapy, which can efficiently kill cancer cells, is able to inhibit the secretion of VEGF simultaneously. Therefore, the combination of antiangiogenic therapy with chemotherapy will mutually enhance each others antitumor effect greatly.[7] However, most of the combination treatment strategies are based on the small molecule drugs, resulting in various significant unfavorable side effects.[2,3b,6b,8a]

Endostar is a modified and recombinant human endostatin, with an additional nine-amino-acid sequence at the N-terminal of the protein to help in protein purification, solubility, activity, and stability.[9] It has been approved by the China Food and Drug Administration for the treatment of non-small-cell lung cancer,[10] and its investigations in other types of cancer, including breast, colon, and pancreatic cancers are under progress.[9] Meanwhile, the combination of endostar and the first-line chemotherapeutic drugs in patients with advanced non-small-cell lung cancer is being studied in clinical trials.[11]

Dr. M. Li, Prof. Z. Tang, Dr. J. Lin, Dr. Y. Zhang, Dr. S. Lv, Dr. W. Song, Prof. X. Chen
Key Laboratory of Polymer Ecomaterials
Changchun Institute of Applied Chemistry
Chinese Academy of Sciences
Changchun 130022, P. R. China
E-mail: xschen@ciac.ac.cn
Dr. M. Li, Dr. J. Lin, Dr. Y. Zhang, Dr. S. Lv
University of Chinese Academy of Sciences
Beijing 100049, P. R. China
Prof. Y. Huang
State Key Laboratory of Polymer Physics and Chemistry
Changchun Institute of Applied Chemistry
Chinese Academy of Sciences
Changchun 130022, P. R. China

DOI: 10.1002/adhm.201400108

Doxorubicin (DOX), an amphiphilic anticancer drug, is a leading clinically used anticancer drug due to its potency and a broad spectrum of activity against diverse cancer types (e.g., breast, lung, prostate, brain, cervix, bone, and bladder cancers).[12] Despite sustained effort over the years, the development of simply synthesized, economical, water-soluble, and biocompatible drug delivery systems with efficient DOX encapsulation is still highly desirable. Carboxymethyl cellulose (CMC), as a commercially available derivative of cellulose, finds widespread use in biomaterials, pharmaceutical formulation, and food.[13a] Due to its excellent biocompatibility, CMC has been approved by the United States Food and Drug Administration (FDA) for parenteral use in drug products such as Sandostatin, Sandolog, and Vivitrol, and is known to be bioeliminable.[13b] Recently, Jiang's group developed a bio-reductive CMC nanogel for DOX delivery, which yielded a significantly superior antitumor effect than the free DOX.[13d]

The purpose of the present study was to investigate the effects of DOX-loaded CMC nanoparticle in combination with endostar for the treatment of non-small-cell lung cancer. To this end, CMC was functionalized with oligo(ethylene glycol), which was neutral in charge and highly hydrophilic, thereby preventing nonspecific protein adsorption on the nanoparticle surface and uptake by the reticuloendothelial system, and providing prolonged blood circulation.[14a] The (2-(2-(2-methoxyethoxy)ethoxy)methyl)oxirane-modified carboxymethyl cellulose (CMC–ME_2MO), synthesized by simply stirring in water solution, could be utilized to efficiently carry DOX (CMC-ME_2MO-DOX) for intracellular delivery with high drug loading and encapsulation efficiency. Compared with free DOX, the resulting CMC-ME_2MO-DOX nanoparticles revealed the delayed and sustained drug release, prolonged blood circulation, improved safety and tolerability, favorable biodistribution, reduced systemic toxicity, and enhanced antitumor efficacy in mice bearing A549 xenograft tumors in vivo, indicating a potential utility in cancer chemotherapy. Furthermore, the antitumor activity of CMC-ME_2MO-DOX in combination with the antiangiogenic drug endostar was also evaluated, which showed a synergistic antitumor effect, implying the optimal therapeutic efficacy in the treatment of non-small-cell lung cancer. Extensive pathological analysis also suggested that the integrated strategy could be exploited as a potential treatment modality for cancer.

2. Results and Discussion

2.1. Synthesis of CMC–ME_2MO

CMC is an FDA-approved polysaccharide-based biomaterial and has been used in a range of biomedical applications because of its wide availability, biocompatibility, and ease of modification.[15a] As shown in **Scheme 1**A, in order to further improve its aqueous solubility, prevent nonspecific protein adsorption, and provide prolonged blood circulation, oligo(ethylene glycol) was conjugated to CMC, by treating CMC with ME_2MO in the alkaline aqueous solution. It has been demonstrated that the irreversible ring-opening conjugation through the primary hydroxyl group and carboxyl group occurred simultaneously in the presence of basic catalyst.[16a] The quantitative ^{1}H NMR spectra of CMC, ME_2MO, and CMC–ME_2MO recorded in D_2O were displayed in **Figure 1**A. After the reaction, the appearance of two peaks at 3.71 and 3.38 ppm and the disappearance of two peaks at 2.96 and 2.78 ppm confirmed the successful conjugation of ME_2MO to the backbone of CMC polysaccharide. The degree of modification (defined as the ratio of ME_2MO units to anhydroglucosidic units) was determined to be 17.9% from the relative integrations of OEGylated proton peaks into carbohydrate protons, which was lower than the design value of 33.3%. This could be explained by the partial hydrolysis of ME_2MO in an aqueous medium. The FT-IR spectrum of CMC–ME_2MO (Figure 1B) clearly revealed the presence of absorbance peak at 1726 cm^{-1} characteristic of ester carbonyl group. The gel permeation chromatography (GPC) trace of CMC–ME_2MO (Figure 1C) was monomodal and quite symmetric, revealing the number average molecule weight ($\bar{M}_n$) of 1.50×10^5 g mol^{-1} and polydispersity index (PDI, $\bar{M}_w/\bar{M}_n$) of 1.85. In comparison with that of CMC (1.32×10^5 g mol^{-1}, PDI = 1.83), GPC trace of CMC–ME_2MO exhibited a clear shift to the higher $\bar{M}_n$ region, indicating that oligo(ethylene glycol) was successfully grafted to the CMC-based precursor. A combination of NMR, FT-IR, and GPC verified the successful synthesis of CMC–ME_2MO with high purity and moderate polydispersity.

2.2. Preparation of the DOX-Loaded CMC–ME_2MO Nanoparticles and In Vitro Drug Release

Conventional systems involving DOX delivery are mostly based on hydrophobic interaction between the drug and hydrophobic moieties of the drug carrier. Organic solvents and other detrimental agents have to be used in this process.[17a] In addition, the hydrophobization treatment on the amphiphilic DOX hydrochloride significantly reduces its anticancer activity.[18] In the present study, the carboxyl groups in the polysaccharide side chain provided sites for complexation with cationic DOX via electrostatic interaction and intermolecular hydrophobic stack in aqueous solution, thus representing a green chemistry approach (Scheme 1B). The drug-loading content (DLC) and drug-loading efficiency (DLE) were calculated to be 16.64 and 99.78 wt%, respectively, indicating high drug encapsulation efficiency.

The scanning electron microscopy (SEM) images showed that both the blank CMC–ME_2MO and DOX-loaded CMC–ME_2MO took a clear spherical morphology, with the average radii of around 38 and 50 nm, respectively (**Figure 2**A,B). In contrast, the hydrodynamic radii measured by DLS were 53 ± 15 (size PDI = 0.085) and 68 ± 21 nm (size PDI = 0.103), respectively (Figure 2C). The smaller size from SEM observations should be due to the dehydration of the nanoparticles in the SEM sample preparation process and the fact that DLS was sensitive to the interference of large particles.[19a] It was believed that the size of DOX-loaded CMC–ME_2MO nanoparticles was optimal for tumor targeting by the enhanced permeability and retention (EPR) effect.[20a]

The in vitro release of DOX from the CMC-ME_2MO–DOX nanoparticles was carried out at pH 7.4 and 5.5 by dialysis method (Figure 2D). The release profiles showed that the

Adv. Healthcare Mater. 2014,
DOI: 10.1002/adhm.201400108

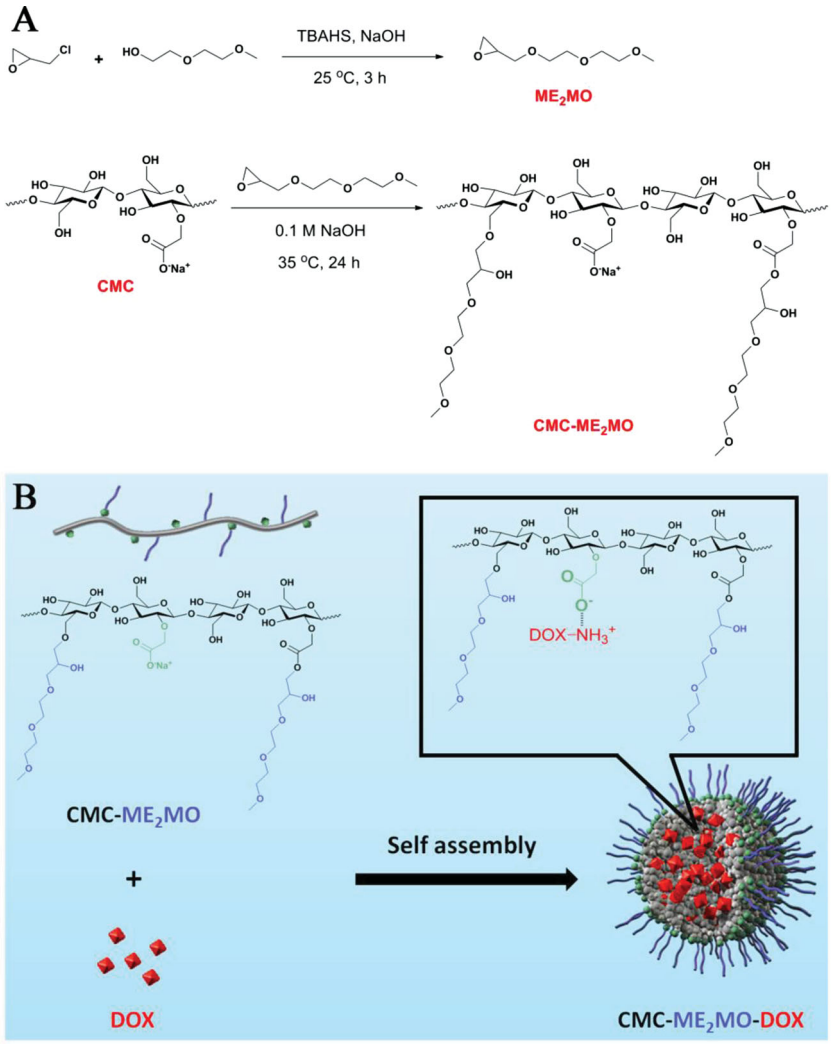

Scheme 1. A) Synthetic routes for the preparation of ME_2MO and CMC–ME_2MO. B) The schematic illustration of the process of preparing CMC-ME_2MO-DOX.

DOX release rate increased as the pH decreased from 7.4 to 5.5, which might be attributed to a significant reduction in the ionization degree of CMC moieties, resulting in extensive disruption of their electrostatic interactions with DOX.[21] In addition, the increased hydrophilicity of DOX in acidic conditions also resulted in a rapid release of DOX.[22] At physiological pH, there was only 36% release for the CMC-ME_2MO-DOX after a 60-h incubation period, while approximately 72% was released at acidic pH. Such a pH-triggered release behavior of DOX showed great potential in drug delivery for the antiproliferative effect, due to the release of DOX in cancer cells while limiting its release in blood circulation.[23a]

2.3. Intracellular Drug Delivery and In Vitro Cytotoxicity

The cellular internalization and intracellular release of DOX were studied in A549 cells by using confocal laser scanning microscopy (CLSM) (**Figure 3**). After 1 h incubation with free DOX and CMC-ME_2MO-DOX, the DOX fluorescence was both found to be aggregated in the cytoplasm and nuclei. When the incubation period was increased to 3 h, stronger DOX fluorescence was observed in cells for both cases. Notably, DOX was found mainly located in the cell nuclei and perinuclear region, and only a small amount of fluorescence was distributed in the cytoplasm for the free DOX group. This could be explained by the rapidly transported of free DOX molecules into the nucleus and avidly bound to the chromosomal deoxyribonucleic acid, after they diffused into the cytosol.[24] In the case of CMC-ME_2MO-DOX, there was still significant DOX fluorescence found in the cytoplasm. This phenomenon had also been observed by other groups before,[25a] ***which was due to the different pathway of internalization. The DOX-loaded nanoparticles were taken into the cells via endocytosis and accumulated in the endosomes where pH-responsive drug release began, followed by the diffusion of DOX into the cytosol and then into the nucleus.[23a,24] The CLSM results demonstrated that the CMC-ME_2MO-DOX nanoparticles were internalized efficiently and DOX could be released in the cytoplasm

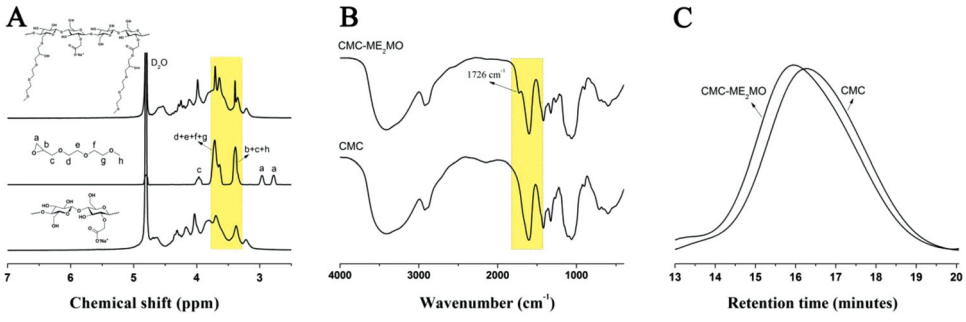

Figure 1. A) ^1H NMR spectra of CMC, ME_2MO, and CMC–ME_2MO in D_2O. B) FT-IR spectra obtained for CMC and CMC–ME_2MO. C) GPC traces recorded for CMC and CMC–ME_2MO.

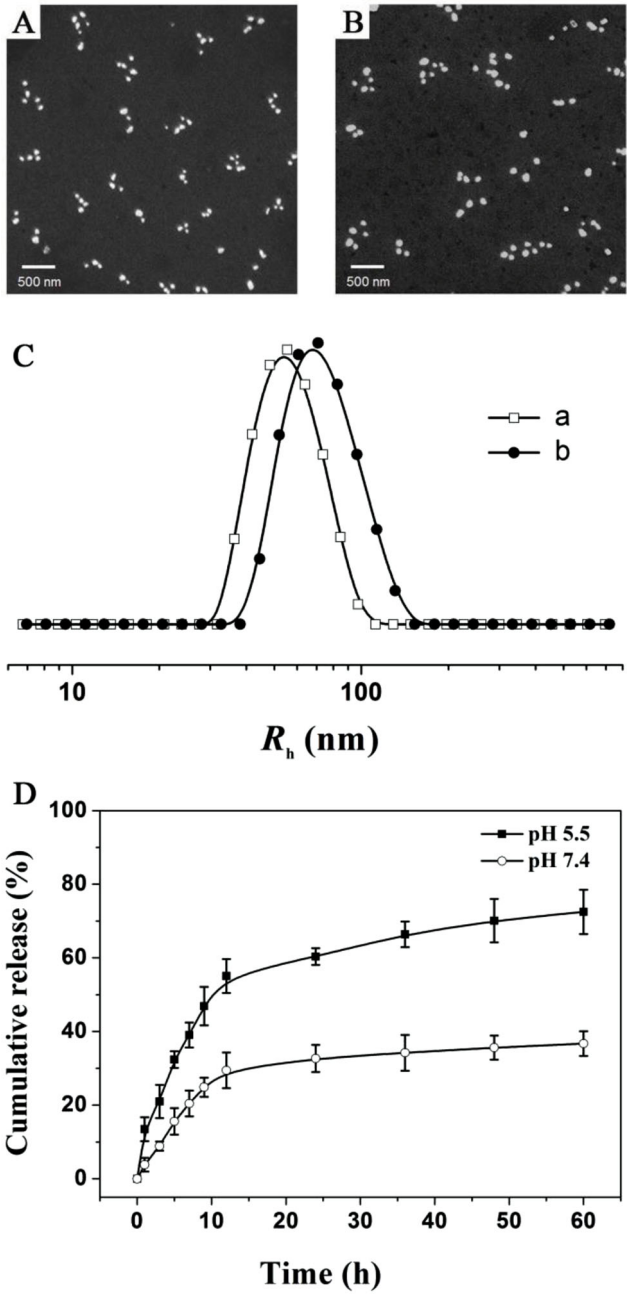

Figure 2. A,B) SEM images of A) CMC–ME_2MO and B) CMC-ME_2MO-DOX. C) Hydrodynamic radius (R_h) distribution of a) CMC–ME_2MO and b) CMC-ME_2MO-DOX. D) Time-dependent cumulative release of DOX from CMC-ME_2MO-DOX nanoparticles at pH 7.4 and 5.5.

and diffused into the nuclei.[25a] It should be noted that the slightly stronger DOX fluorescence was observed in cells following incubation with free DOX for 1 and 3 h, compared with CMC-ME_2MO-DOX. This could be attributed to the slightly slower cellular uptake of DOX-loaded nanoparticles and delayed drug release from the CMC-ME_2MO-DOX nanoparticles,[26a] which was consistent with the results obtained in buffered solutions (Figure 2D). For further confirmation, the cellular uptake of free DOX and CMC-ME_2MO-DOX into the A549 cells was analyzed using fluorescence-activated flow cytometry (Figure S1 and S2, Supporting Information), and the consistent results were acquired.

In order to assess whether the DOX-loaded nanoparticles enter cells via endocytosis, we incubated cells with fluorescein isothiocyanate (FITC)-labeled CMC-ME_2MO-DOX and compared the fluorescence distributions of FITC and DOX in the cells via CLSM analysis. As shown in Figure S3 (Supporting Information), the FITC-labeled CMC–ME_2MO nanoparticles (green fluorescence) were mainly dispersed in the cytoplasm of A549 cells, but not in the nucleus, which was stained into blue. It was also noted that the DOX molecules that released from the nanoparticles could be accumulated in the nucleus, suggesting the DOX release from the nanoparticles. This result indicated that the DOX-loaded nanoparticles were taken up by A549 cells via endocytosis.[13d,18]

Cytotoxicity was also a crucial issue that needed to be addressed before the drug delivery vector was utilized for in vivo tumor chemotherapy. The biocompatibility studies using A549 cells revealed that CMC–ME_2MO was nontoxic up to the highest testing concentration of 1.0 g L^{-1} (**Figure 4**A), indicating its excellent biocompatibility. At an equivalent drug concentration, CMC-ME_2MO-DOX nanoparticles revealed a slightly lower antitumor activity as compared to free DOX after incubation for 24 and 48 h (Figure 4B). It was due to free DOX of an amphipathic small molecule that could easily diffuse across the cell membrane, while the CMC-ME_2MO-DOX nanoparticles were internalized through the endocytic compartment to enter the cell and the loaded drug was slowly released from the carriers, thus resulting in the lower cytotoxic efficiency of CMC-ME_2MO-DOX.[27a]

2.4. Hemolysis and Pharmacokinetics

It was important to guarantee the blood compatibility of the drug carrier, because it would be finally injected intravenously into blood vessels. In the present study, the hemolytic behavior of CMC–ME_2MO was investigated, using triton X-100 and Phosphate buffered saline (PBS) as the positive and negative control, respectively. As shown in **Figure** 5A, triton X-100 exhibited significant hemolysis, whereas CMC–ME_2MO showed negligible hemolysis toxicity (≈0%) to RBCs even at the highest polymer concentration of 5.0 g L^{-1}, demonstrating the excellent blood compatibility of CMC–ME_2MO and the potential application as drug delivery vehicles.

The stability and long circulation capability of drug-loaded nanoparticles in blood were an important issue for effective drug redistribution to the tumor site. Here, plasma pharmacokinetics of free DOX and CMC-ME_2MO-DOX formulations were evaluated with high performance liquid chromatography (HPLC) from rat plasma after intravenous administration. As shown in Figure 5B, the disappearance of free DOX as well as CMC-ME_2MO-DOX from blood circulation compartment occurred in a biexponential manner, whereas the plasma DOX concentration of CMC-ME_2MO-DOX was slightly higher than free DOX. After the intravenous injection of free DOX and CMC-ME_2MO-DOX, the maximum plasma concentration (C_{max}) and clearance rate (CL) were 3945 ± 933 and

DOI: 10.1002/adhm.201400108

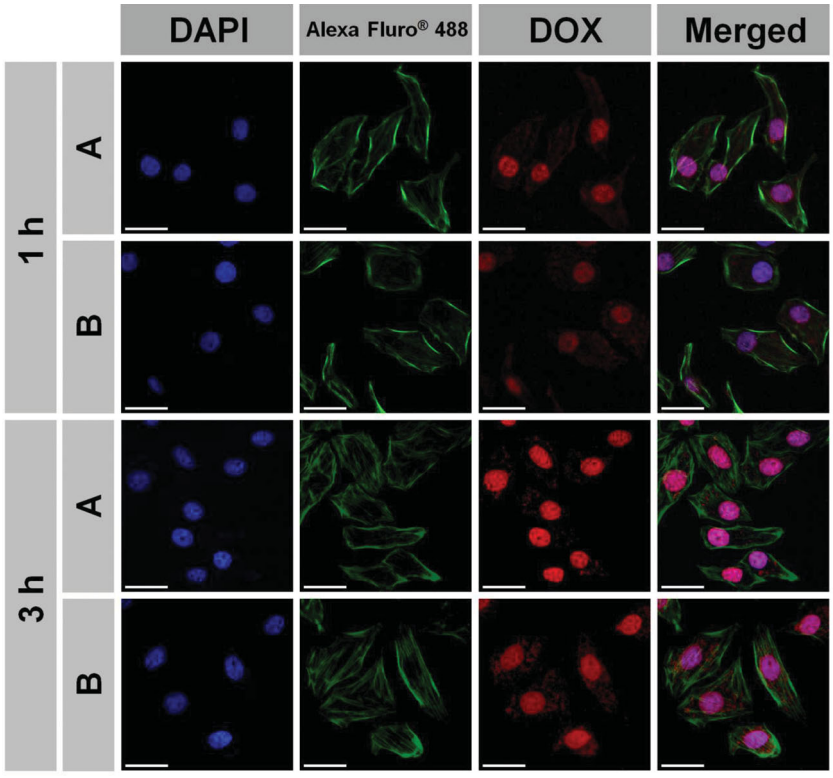

Figure 3. Cellular uptake of A) free DOX and B) CMC-ME_2MO-DOX after incubation with A549 cells for 1 and 3 h, observed by CLSM. DAPI (4′,6-diamidino-2-phenylindole dihydrochloride, blue) and Alexa Fluor 488 phalloidin (green) were used to stain cell nuclei and cytoskeleton, respectively. The scale bars represent 30 μm.

4986 ± 1158 ng mL^{-1}, 140 ± 30 and 111 ± 8 mL min^{-1} kg^{-1}, respectively. The area under the plasma concentration–time curve from time zero to the last measurable sample time (AUC_{0-t}) was 95850 ± 16378 and 143712 ± 7817 ng min mL^{-1}, respectively.

2.5. In Vivo Toxicity and Tolerability

To determine the toxicity and tolerability, the maximum tolerated dose (MTD) for a single intravenous administration of the blank drug carrier and DOX-loaded CMC–ME_2MO nanoparticles was assessed in Kunming mice and compared to free DOX. The body weight and survival details of the mice were monitored for 10 d after injection of CMC–ME_2MO at doses of 0, 50, 100, 150, and 200 mg kg^{-1}, and free DOX and CMC-ME_2MO-DOX at doses of 5, 10, 15, 20, and 25 mg kg^{-1} DOX equivalents (**Table 1** and Figure S4, Supporting Information).

No morbidity, death or weight loss was observed for CMC–ME_2MO at doses up to 200 mg kg^{-1}, indicating its excellent biocompatibility and a potential clinical utility. As shown in Table 1, free DOX was well tolerated at the dose of 5 mg kg^{-1}. However, increasing the DOX dosage to 10 mg kg^{-1} resulted in the death of two mice among the three treated mice. A significant body weight loss was observed at 15, 20, and 25 mg kg^{-1} of free DOX, and all the mice in the groups treated with doses higher than 15 mg kg^{-1} died within 4 d post-injection (Figure S4C and S4D, Supporting Information). For the mice treated with the DOX-loaded CMC–ME_2MO nanoparticles, there were no significant body weight loss and noticeable changes in normal activity at a DOX dosage of 10 mg kg^{-1} (Figure S4E and S4F, Supporting Information). Further increase of the dosage above 15 mg kg^{-1}, however, resulted in the death of the treated mice. Noteworthy, intravenous injection of CMC-ME_2MO-DOX formulation resulted in a substantially prolonged mean survival time as compared to the free DOX at the same doses (Table 1). The MTD was estimated based on the threshold at which all animals survived and the body weight loss was below 20%.[28] The corresponding MTD of free DOX was determined to be 5 mg kg^{-1}, which was in accordance with previous studies.[29] However, DOX-loaded CMC–ME_2MO nanoparticles were able to increase the MTD of DOX from 5 to 10 mg kg^{-1}, which was likely due to the delayed drug release and decreased nonselective uptake by major organs. The improved safety of CMC–ME_2MO nanoparticles-mediated DOX delivery suggested that CMC-ME_2MO-DOX might allow a full dose of chemotherapy without the limiting toxicities.

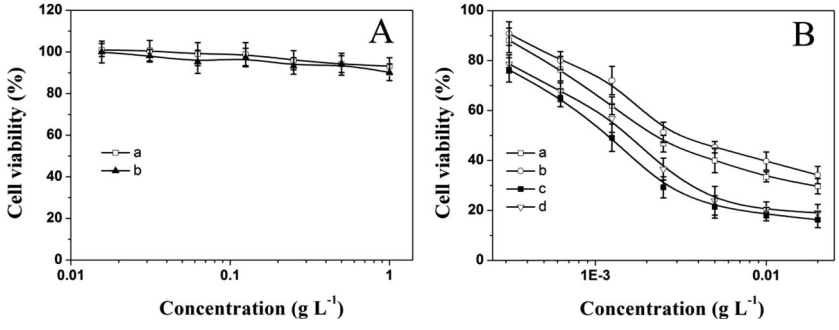

Figure 4. A) Viability of A549 cells after treatment with CMC–ME_2MO for a) 24 and b) 48 h. B)In vitro cytotoxicities of a,c) free DOX and b,d) CMC-ME_2MO-DOX to A549 cells after incubation for a,b) 24 and c,d) 48 h.

2.6. Ex Vivo DOX Fluorescence Imaging

Biodistribution of free DOX and CMC-ME_2MO-DOX nanoparticles after systemic administration was evaluated with ex vivo imaging studies. At 3, 10, and 24 h post-injection, imaging of the isolated visceral organs and tumors was carried out in nude mice bearing A549 tumor. The fluorescence intensity of DOX was represented in **Figure 6**A in terms of a color

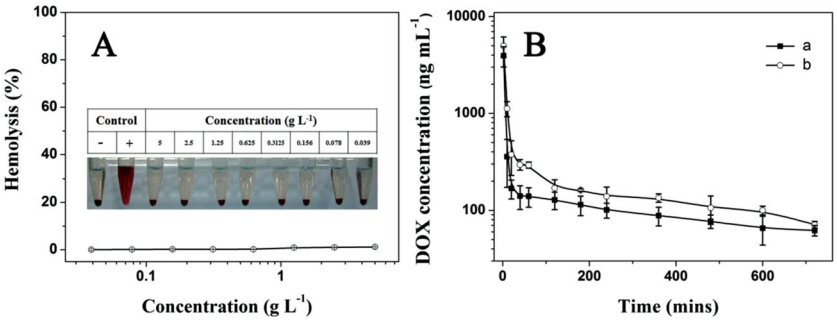

Figure 5. A) Hemolytic activity of CMC–ME_2MO. PBS and triton X-100 (10 g L^{-1}) were used as negative and positive controls, respectively. B)In vivo pharmacokinetics profiles after intravenous injection of a) free DOX and b) CMC-ME_2MO-DOX in rats. Data are presented as a mean ± standard deviation (n = 3).

scale and semi-quantitatively analyzed in Figure 6B. At 3 h post-injection, kidney and liver showed strong fluorescence intensity for free DOX group, suggesting that the drug molecules as foreign bodies were mainly eliminated and metabolized by the kidney and the liver.[30] However, the fairly weaker fluorescence in the kidney for the injection of CMC-ME_2MO-DOX was observed, compared with free DOX, which might be due to the improved pharmacokinetics and enhanced reinforced blood stability of the nanomedicine formulations. The photon numbers per unit area (average signals) shown in Figure 6B indicated that, the fluorescence intensities at tumor sites for CMC-ME_2MO-DOX nanoparticles were stronger than those of free DOX during the whole experimental period, that were, 1.14-, 1.56-, and 1.30-fold higher than those at 3, 10, and 24 h post-injection, respectively. Interestingly, the fluorescence signal of CMC-ME_2MO-DOX at tumor site increased at the first 10 h, and followed by a slight decrease at 24 h. This might be attributed to the deeper penetration in tumor tissue for CMC-ME_2MO-DOX with time, which resulted in the fluorescence intensity decrease.[31] These data confirmed that the CMC-ME_2MO-DOX nanoparticles increased accumulation in tumor over time, which could further contribute to increase the cancer therapy efficiency by EPR effect.[32] Equally important, the CMC-ME_2MO-DOX nanoparticles significantly reduced the location of DOX in the heart, as compared to the free DOX. This indicated that the use of CMC–ME_2MO as a DOX carrier could minimize the possibility of DOX-associated side effects in the heart, such as cardiomyopathy and congestive heart failure.[33] An improved biodistribution with increased and decreased accumulation in tumor and the normal tissues (especially for heart and kidney), respectively, for the injection of CMC-ME_2MO-DOX indicated that the DOX-loaded nanoparticles were able to alter the biodistribution of the drug and contribute to enhance the tumor accumulation and reduce the drug's systemic toxicity.

2.7. In Vivo Anticancer Efficacy

Based on the appropriate physicochemical properties, sustained drug release behavior, prolonged blood circulation, and enhanced tumor localization, the potential of CMC-ME_2MO-DOX in combination with endostar for the treatment of non-small-cell lung cancer was further explored. The antitumor efficacy was investigated on Balb-c/nude mice bearing A549 tumors. To provide in vivo evidence for the antitumor potential of CMC-ME_2MO-DOX nanoparticles, the treatments were done by intravenously injecting PBS, free DOX (3.0 mg kg^{-1}) and

Table 1. Dosing information of CMC–ME_2MO, free DOX, and CMC-ME_2MO-DOX for MTD studies in Kunming mice.

Groups	Dose [mg kg^{-1}]	Number of mice	Number of death	Mean survival time [d]	Percent of body weight at day 10 [%]
PBS	–	3	0	10.0	134.2 ± 15.3
CMC–ME_2MO	50	3	0	10.0	134.2 ± 11.5
	100	3	0	10.0	131.4 ± 7.7
	150	3	0	10.0	128.8 ± 9.7
	200	3	0	10.0	125.9 ± 13.8
Free DOX	5	3	0	10.0	125.8 ± 12.2
	10	3	2	6.0 ± 3.6	97.1
	15	3	3	3.0	–
	20	3	3	3.0	–
	25	3	3	2.7 ± 0.6	–
CMC-ME_2MO-DOX	5	3	0	10.0	124.6 ± 6.3
	10	3	0	10.0	105.0 ± 10.2
	15	3	1	8.3 ± 2.9	102.2 ± 7.3
	20	3	3	4.7 ± 0.6	–
	25	3	3	4.0 ± 1.0	–

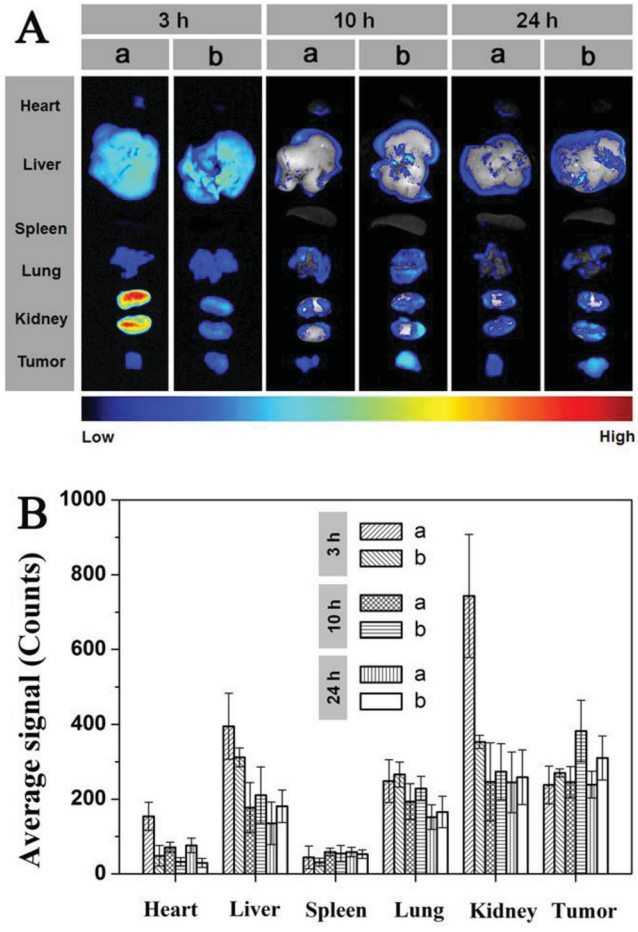

Figure 6. A) Ex vivo DOX fluorescence images showing the drug bio-distribution of a) free DOX and b) CMC-ME_2MO-DOX in nude mice bearing A549 tumor at 3, 10, and 24 h post-injection. B) Average signals collected from the major organs (heart, liver, spleen, lung, and kidney) and tumors after the treatment of a) free DOX and b) CMC-ME_2MO-DOX at different time points.

CMC-ME_2MO-DOX (3.0 mg kg^{-1} DOX eq.), respectively, into tumor-bearing mice. Furthermore, the antitumor activity of free DOX (3.0 mg kg^{-1}) or CMC-ME_2MO-DOX (3.0 mg kg^{-1} DOX eq.) in combination with the approved antiangiogenic drug endostar (8.0 mg kg^{-1}) was also evaluated. It has been reported that rational drug scheduling plays an important role in combination cancer therapy, which may result in optimized therapeutic effect.[6b,34] Previous studies demonstrated that endostar given simultaneously with or following chemotherapeutic drug might be optimal to enhance the antitumor effect.[34,35] In this study, endostar was injected 1 h after the treatment of free DOX or CMC-ME_2MO-DOX.

As shown in **Figure 7**A, compared with the control group (group a), the tumor growth was slightly delayed in endostar group (group c), and effectively inhibited in all the groups containing the chemotherapeutics (group b, d, e, and f, $^{***}p < 0.001$, compared with group a). The CMC-ME_2MO-DOX nanoparticles (group e) displayed enhanced inhibition of tumor growth in comparison to free DOX (group b), which might be explained by the enhanced accumulation of the nanoparticles at the tumor site. Furthermore, the effective encapsulation of DOX against leakage in the bloodstream and the facilitated intracellular release of DOX might also contribute to the observed enhanced antitumor efficacy.[36] It is of interest to note that the combination therapy groups (group d, free DOX plus endostar; group f, CMC-ME_2MO-DOX plus endostar) showed the obviously enhanced antitumor efficacy, compared with the groups treated with free DOX (group b) and CMC-ME_2MO-DOX (group e), respectively. Remarkably, the CMC-ME_2MO-DOX plus endostar group (group f) showed the highest efficacy in tumor suppression compared to the other groups ($^{\#}p < 0.05$, compared with CMC-ME_2MO-DOX), which indicated that the fusion of two kinds of treatments led to a significant benefit relative to the use of each method alone. It relied on the synergistic effects of the chemotherapy and antiangiogenic therapy as explained in **Scheme 2**. The DOX molecules released from CMC-ME_2MO-DOX contributed to the chemotherapeutic efficacy, while the endostar could effectively prevent the formation of the tumor blood vessels, resulting in the additional inhibition of tumor growth. At day 18 post-injection, the tumor suppression rates of endostar (group c), free DOX (group b), free DOX plus endostar (group d), CMC-ME_2MO-DOX (group e), and CMC-ME_2MO-DOX plus endostar (group f) were 23.5%, 65.9%, 76.1%, 78.9%, and 89.5%, respectively.

All the mice were alive during the experimental period. In particular, after 18 d, the CMC-ME_2MO-DOX treatment resulted in almost no difference in the physical activity level and body weight. Compared with the CMC-ME_2MO-DOX group, there was a slight loss of body weight in mice receiving free drug treatment (5.8% body weight loss at day 18, Figure 7B). However, for the control (group a) and endostar (group c), the continuous tumor growth resulted in sustained increase of body weight (approximately 8.5% body weight gain at day 18).

2.8. Histological and Immunohistochemical Analyses

To further evaluate the antitumor efficacy after treatment with various formulations, the tumors and major organs (heart, liver, spleen, lung, and kidney) were dissected from mice and sectioned for pathology analysis. As shown in Figure 7C, in the control and endostar groups (group a and c), the tumor tissue sections were composed of tightly packed tumor cells interspersed with various amounts of stroma. The tumor cells with a large nucleus and a spherical or spindle shape were observed, in which more binucleolates and chromatin were also observed, indicating a rapid tumor growth. However, the tumors treated with all the DOX-involved formulations (group b, d, e, and f) exhibited significantly different histological features. The tumor cells displayed enlarged sizes and excessive vacuolization, with various degrees of tissue necrosis, extensive nuclear shrinkage, and fragmentation. Additionally, many of the tumor cells were composed of membrane-bound, small nuclear fragments surrounded with a rim of cytoplasm, exhibiting typical apoptotic characteristics.[37] Especially for the CMC-ME_2MO-DOX plus endostar-treated tumor cells, chromatin was concentrated and distributed around the edge, and nuclei

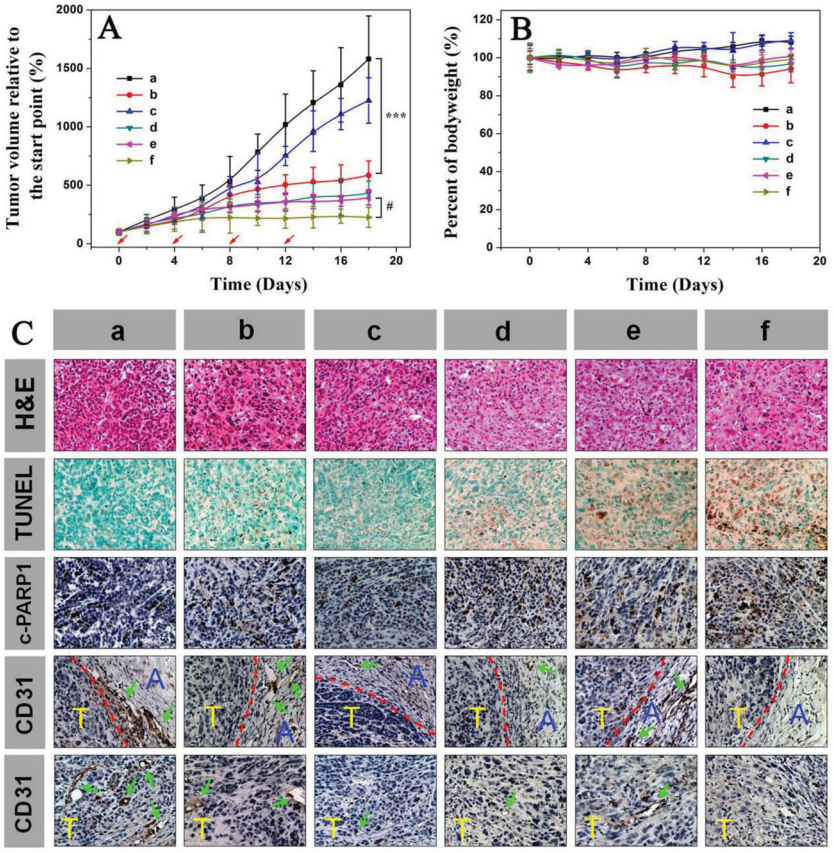

Figure 7. In vivo antitumor efficacy and histological observation of tumors after the treatment of a) PBS, b) free DOX (3.0 mg kg^{-1}), c) endostar (8 mg kg^{-1}), d) free DOX (3 mg kg^{-1}) plus endostar (8 mg kg^{-1}), e) CMC-ME_2MO-DOX (3.0 mg kg^{-1} DOX eq.), and f) CMC-ME_2MO-DOX (3.0 mg kg^{-1} DOX eq.) plus endostar (8 mg kg^{-1}) in the A549 tumor-bearing mouse model. A) Tumor sizes of the mice as a function of time. The arrows represent the day on which the intravenous tail vein injection was performed. B) Body weight changes with the time of tumor-bearing mice. C) Ex vivo histological, TUNEL, and immunohistochemical analyses of A549 tumor sections (18 d after the first treatment). Nuclei were stained bluish violet, whereas extracellular matrix and cytoplasm were stained pink in staining. Brown and green stains indicated apoptotic and normal cells, respectively, in TUNEL analysis. Brown and blue stains indicated cleaved PARP1 (or blood vessel, detected by CD31-specific antibody) and nuclei, respectively, in immunohistochemical assay. In CD31 immunohistochemical assay: red dashed line separated boundary of tumor tissue (T) and adjacent tissue (A); green arrows pointed to the blood vessels.

became pyknotic, fragmented or absence, and the necrosis area was the largest among the tested groups. As shown by the TUNEL assay, tumors treated with all the DOX formulations had extensive regions of apoptotic cells, especially for CMC-ME_2MO-DOX and its combination with endostar-administrated tumors, whereas such apoptotic cells were much less present in the tumors treated with only endostar or PBS, which was consistent with the in vivo antitumor capability and hematoxylin and eosin (H&E) stain results. Meanwhile, the level of cleaved 25 kDa fragment of PARP1, one of the essential substrates cleaved by both caspase-3 and -7,[38a] was significantly elevated in the CMC-ME_2MO-DOX group (group e) and its combination with endostar (group f), indicating that more cells underwent apoptosis in these groups.

The effect of endostar on tumor neoangiogenesis was further investigated by immunohistochemical staining with anti-CD31 antibody to visualize tumor blood vessels in the tumor and adjacent tissue. As shown in Figure 7C, the tumors treated with PBS were highly vascular, with many large blood vessels and microvessels located in the tumor and its adjacent tissue, consistent with the continuous tumor growth. As expected, the single chemotherapeutic drug-administrated groups (group b, free DOX; group e, CMC-ME_2MO-DOX) showed a reduced number of microvessels in the tumor tissues, compared with the control group (group a, PBS), indicating that free DOX could inhibit angiogenesis in some extent. This result was consistent with what has been previously reported.[39a] VEGF, which was overexpressed and secreted mostly by tumor cells, could efficiently stimulate proliferation of endothelial cells and cause angiogenesis in tumor tissue. However, chemotherapeutic drugs, which could efficiently kill cancer cells, were also able to inhibit the secretion of VEGF simultaneously.[40a] Notably, endostar (group c) and its combination with free DOX (group d) suppressed new blood vessels development not only in the tumors, but also in the surrounding areas. Remarkably, the CMC-ME_2MO-DOX plus endostar-treated tumors showed the largest decrease in CD31-positive microvessels, compared with all the other groups, consistent with the results of antitumor effects.

Together, these results demonstrated that CMC-ME_2MO-DOX could efficiently deliver DOX to the tumor, leading to reduced cell proliferation and increased apoptosis in vivo. The combination of CMC-ME_2MO-DOX and endostar strongly enhanced the antitumor and antiangiogenic efficacies in A549 tumor-bearing mice models.

Furthermore, the representative sections of the main organs including heart, liver, spleen, lung, and kidney taken at day 18 from control mice receiving PBS and mice receiving various drug formulations were stained by H&E (**Figure 8**). Histological slices in spleen, lung, and kidney revealed that free DOX (group b), endostar (group c), CMC-ME_2MO-DOX (group e), and their combinations (group d and f) revealed no significant signal of organ damage and did not cause any inflammatory response, degeneration, or necrosis. Nevertheless, varying degrees of heart, and liver damages were observed from H&E-stained organ slices in all the DOX involved groups (group b, d, e, and f). Obvious cardiotoxicity was induced by free DOX-treated groups (group b and d) due to the observed hyperemia, myocardial fiber breakage with acute inflammatory cell infiltration, critical pathological changes, and necrosis of the muscle fibers in cardiac tissues. In contrast, the treatment of tumor-bearing mice by DOX-encapsulated CMC–ME_2MO nanoparticles obviously reduced the blight of heart. This was in

Adv. Healthcare Mater. **2014**,
DOI: 10.1002/adhm.201400108

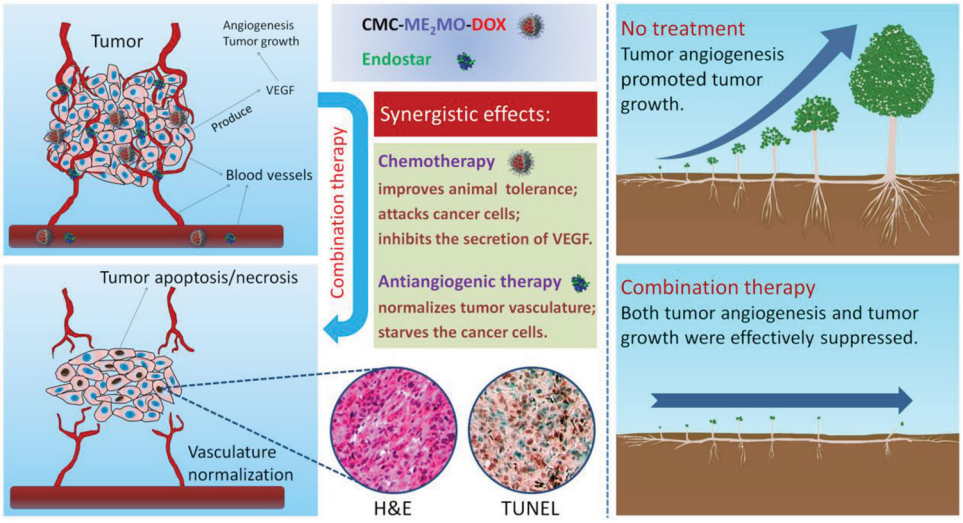

Scheme 2. Schematic diagram of mechanisms and synergistic therapeutic effects based on the combination of chemotherapeutic nanomedicine (CMC-ME_2MO-DOX) and antiangiogenic drug (endostar).

accordance with the results of biodistribution study (Figure 6), in which the accumulation of the CMC-ME_2MO-DOX in heart was found relatively lower than free DOX. On the other hand, the delayed drug release of DOX from the carriers during the blood circulation might also contribute to the decreased cardiotoxicity. Although slight structural disturbance with microregional necrosis of hepatocytes could be observed in the liver for both free DOX- and CMC-ME_2MO-DOX-treated groups, the fast liver regeneration with healthy hepatocytes could help the animals for effective recovery from the metabolic break.[41a]

3. Conclusions

We have demonstrated that the DOX-loaded OEGylated CMC nanoparticles efficiently delivered DOX into A549 lung cancer cells in vitro and reduced A549 xenograft tumor size in vivo. CMC–ME_2MO could not only be easily synthesized by simply stirring in water solution, but also efficiently carry DOX with high drug loading and encapsulation efficiency (nearly 100%) through the electrostatic interaction and intermolecular hydrophobic stack. Importantly, the encapsulation of DOX in

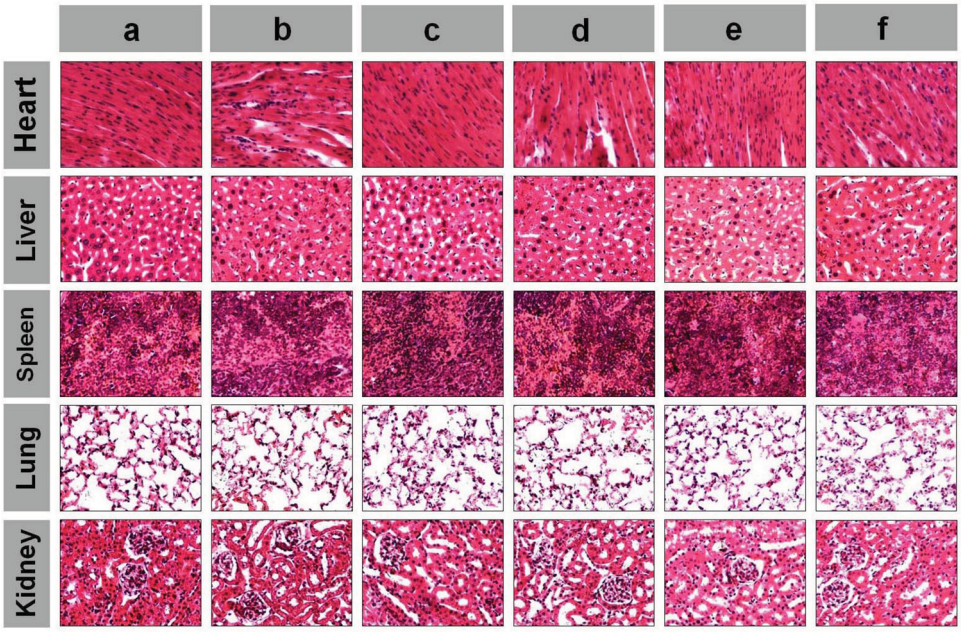

Figure 8. Histologic assessments of major organs with H&E staining in mice. The organs were harvested from A549 tumor-bearing mice at day 18, after the quartic intravenous injection of a) PBS, b) free DOX, c) endostar, d) free DOX plus endostar, e) CMC-ME_2MO-DOX, and f) CMC-ME_2MO-DOX plus endostar.

the CMC–ME_2MO nanoparticles significantly improved the tolerability, in vivo pharmacokinetics, biodistribution, and antitumor efficacy. Furthermore, we also evaluated the antitumor activity of CMC-ME_2MO-DOX in combination with the approved antiangiogenic drug endostar, which showed the highest efficiency in tumor reduction (TSR, 89.5%) and antiangiogenesis. To the best of our knowledge, this was the first report on the synergy of DOX-loaded nanoparticles and endostar for the therapy of non-small-cell lung cancer, based on the study of tumor growth suppression in vivo. It is demonstrated that the combinational chemotherapy and antiangiogenic therapy strategy exhibited a remarkably synergistic antitumor effect that was greater than the two treatments alone. With the convenient fabrication, reliable safety and flexible dosing regimen, this combination of CMC-ME_2MO-DOX and endostar held great potential for achieving an optimal therapeutic effect in the clinical treatment of non-small-cell lung cancer.

4. Experimental Section

Materials: Sodium carboxymethyl cellulose (CMC, M_W = 90 K, degree of substitution (DS) = 0.7 carboxymethyl group per anhydroglucose unit, Aldrich), tetrabutylammonium hydrogen sulfate (TBAHS, 99%; Aldrich), 2-(2-methoxyethoxy)ethanol (98%; Aldrich), epichlorohydrin (J&K Chemicals), doxorubicin hydrochloride (99%; Beijing Huafeng United Technology Corporation), recombinant human endostar (Simcere, China), 3-(4,5-Dimethyl-thiazol-2-yl)-2,5-diphenyl tetrazolium bromide (MTT; Sigma), FITC (Aladdin, Shanghai, China), and 4′,6-diamidino-2-phenylindole dihydrochloride (DAPI; Sigma) were used without further purification. Purified deionized water was prepared by the Milli-Q plus system (Millipore Co., Billerica, MA, USA).

Measurements: ^{1}H NMR spectra were recorded on a Bruker AV 400 NMR spectrometer in D_2O. GPC analyses of CMC and CMC–ME_2MO were conducted on a Waters 2414 system equipped with Ultrahydrogel linear column and a Waters 2414 refractive index detector (eluent: 0.1 M phosphate buffer, pH 7.4; flow rate: 0.5 mL min^{-1}; temperature: 35 °C; standard: poly(ethylene glycol)). Dynamic laser scattering (DLS) measurement was performed on a WyattQELS instrument with a vertically polarized He–Ne laser (DAWN EOS, Wyatt Technology). UV–vis absorption spectra were recorded on a Shimadzu UV-2401PC UV–vis spectrophotometer. SEM images were obtained with a Hitachi S-4800 FE-Scanning electron microscope.

Synthesis of CMC–ME_2MO: ME_2MO was synthesized according to the previously described synthetic method.[14a] ME_2MO-decorated carboxymethyl cellulose (CMC–ME_2MO) was obtained by reaction of CMC with ME_2MO in aqueous NaOH.[16a,c] Briefly, CMC (2.001 g) was dissolved in 50 mL of 0.1 M NaOH solution, followed by addition of ME_2MO (0.5365 g, 3.0447 mmol). The reaction was performed at 35 °C for 24 h. The product was isolated by precipitation in cold ethanol and dried under vacuum. The resulting white powder was then dissolved in deionized water, dialyzed against deionized water for 3 d. The final product was obtained as a white cake-like solid after lyophilization of the dialyzed solution.

In Vitro Drug Loading and Release: CMC–ME_2MO lyophilized powder was dissolved in deionized water and stirred for 10 min, then adjusted pH to 7.4. An aqueous solution of doxorubicin hydrochloride was added dropwise into the polymer solution and the mixture solution was vigorously stirred overnight in the dark. Excess drug was removed by dialysis against deionized water for 24 h and followed by lyophilization in the dark. The DLC and DLE of DOX were determined by using UV–vis spectrometer. DLC and DLE were calculated according to the following formula:

$$\text{DLC(wt\%)} = (\text{weight of loaded drug/weight of drug} - \text{loaded nanoparticles}) \times 100\%$$

$$\text{DLE(wt\%)} = (\text{weight of loaded drug/weight of feeding drug}) \times 100\%$$

FITC-labeled CMC-ME_2MO-DOX nanoparticles were prepared by a two-step method. First, CMC–ME_2MO was labeled with FITC. Briefly, 5 mg FITC dissolved in 2 mL of dimethyl sulfoxide was slowly drop-wise added to 2 mg mL^{-1} CMC–ME_2MO (30 mg) dissolved in Milli-Q-grade water. The mixture solution was vigorously stirred for another 12 h in the dark, and then purified by dialysis against deionized water for 24 h. A light yellow powder was obtained after lyophilization. Second, DOX was loaded into FITC-labeled CMC–ME_2MO by the same procedure described above. To avoid interference from FITC, DLC, and DLE of DOX were determined by a scanning spectrofluorimeter (Photon Technology International, Birmingham, NJ) using a standard curve method (the excitation and emission wavelengths were 472 and 592 nm, respectively). To determine the release profiles of DOX, the weighed freeze-dried DOX-loaded nanoparticles were suspended in 10.0 mL of release medium and transferred into a dialysis bag (MWCO 3500 Da). The release experiment was initiated by placing the end-sealed dialysis bag into 45.0 mL of release medium at 37 °C with constant shaking. At selected time intervals, 3.0 mL of release media was taken out and replenished with an equal volume of fresh media. The amount of DOX released was determined using UV–vis spectrometer at 480 nm using the standard curve method.

Cell Cultures: The human lung carcinoma (A549) cells were cultured at 37 °C in a 5% CO_2 atmosphere in Dulbecco's modified Eagle's medium (DMEM, Gibco) supplemented with 10% fetal bovine serum (FBS), penicillin (50 U mL^{-1}), and streptomycin (50 U mL^{-1}).

Confocal Laser Scanning Microscopy Observation: The cellular uptake and intracellular release behaviors of CMC-ME_2MO-DOX were determined by CLSM toward A549 cells. The cells were seeded on the coverslip in six-well plates with a density of 1×10^5 cells per well in 2 mL of DMEM and cultured for 24 h, and then the original medium was replaced with free DOX, or CMC-ME_2MO-DOX (at a final DOX concentration of 5 mg L^{-1}) containing DMEM. After 1 and 3 h incubation, the cells were washed and fixed with 4% formaldehyde for 20 min at room temperature. Then, the cells were counterstained with DAPI for cell nucleus and Alexa Fluor 488 phalloidin (Invitrogen, Carlsbad, CA) for cytoskeleton following the manufacturer's instructions. The cellular localization was visualized under a laser scanning confocal microscope (Carl Zeiss, LSM 780). The cellular internalization and the accumulation of FITC-labeled CMC-ME_2MO-DOX were monitored by CLSM. Briefly, A549 cells were incubated with the FITC-labeled CMC-ME_2MO-DOX nanoparticles at 37 °C for 1.5 h, and then the cells were washed, fixed with 4% formaldehyde, and stained with DAPI for cell nuclei.

Cellular Uptake Measured by Flow Cytometry: A549 cells were seeded in six-well plates with a density of 3×10^5 cells per well in 2 mL of DMEM and incubated for 24 h, and then the original medium was replaced with free DOX or DOX·HCl-loaded NPs (at a final DOX concentration of 5 mg L^{-1}) containing DMEM. The cells were incubated for 1 and 3 h at 37 °C, and then washed three times with PBS. The harvested cells were suspended in PBS and centrifuged at 1200 rpm for 4 min at 4 °C. The supernatants were discarded and the cells were washed with PBS to remove the background fluorescence in the medium. After three cycles of washing and centrifugation, cells were resuspended with 400 µL of PBS, and flow cytometry analysis was done using a Becton Dickinson FACSCalibur cytometer equipped with an argon laser (488 nm) and emission filter for 570 nm (Cytomics FC 500, Beckmann-Coulter).

Cytotoxicity Assay: The cytotoxicities of CMC–ME_2MO, free DOX, and CMC-ME_2MO-DOX were evaluated by MTT assay. The cells were seeded in 96-well plates (1×10^4 cells per well) in 100 µL of DMEM medium and incubated at 37 °C in a 5% CO_2 atmosphere for 24 h. The culture medium was replaced with 200 µL of fresh medium containing CMC–ME_2MO, free DOX, and CMC-ME_2MO-DOX. The cells were subjected to MTT assay after being incubated for another 24 h. The absorbency of the

DOI: 10.1002/adhm.201400108

solution was measured on a Bio-Rad 680 microplate reader at 490 nm. The relative cell viability was determined by comparing the absorbance at 490 nm with control wells containing only cell culture medium. Data are presented as means ± SD ($n = 6$).

Hemolysis Assay: Hemolytic activity of CMC–ME_2MO was evaluated according to the previous protocol with minor modification.[42] PBS and triton X-100 (10 g L^{-1}), a surfactant known to lyse red blood cells (RBCs), were used as negative and positive controls, respectively. The hemolysis ratio of RBCs was calculated using the following formula: hemolysis (%) = $(A_{sample} - A_{negative\ control})/(A_{positive\ control} - A_{negative\ control}) \times 100$, where A_{sample}, $A_{negitive\ control}$, and $A_{positive\ control}$ were denoted as the absorbencies of samples, negative and positive controls, respectively. All hemolysis experiments were carried out in triplicates.

Pharmacokinetics: Female Wistar rats (240–250 g, provided by Laboratory Animal Center of Jilin University) were randomly divided into two groups ($n = 3$). Free DOX and CMC–ME_2MO were administered intravenous via tail vein (5 mg kg^{-1} on DOX basis). At defined time periods (2, 10, 20, 40, 60, 120, 180, 240, 360, 480, 600, and 720 min), blood samples were collected from orbital cavity, heparinized, and centrifuged to obtain the plasma. The concentrations of DOX in the above samples were determined by the HPLC methods reported previously with minor modifications.[43a] Briefly, a 180 µL plasma sample was deproteinized with 600 µL of acetonitrile, 200 µL of methanol, and 100 µL of daunorubicin hydrochloride (1 µg mL^{-1}, internal standard), vortexed for 10 min, and centrifuged at 13 000 rpm for 10 min. Then, 800 µL of supernatant was collected and dried under a stream of nitrogen at 35 °C. The dried sample was then dissolved in the mobile phase for HPLC analysis. Waters liquid chromatographic system (Waters e2695 Separations Module, USA) was equipped with a fluorescence detector (Waters 2475 Multi λ Fluorescence Detector, USA) with the excitation and emission wavelengths set at 472 and 592 nm, respectively. A Waters Symmetry C18 analytical column (5 µm, 4.6 × 250 mm) was used at 35 °C. The pharmacokinetic parameters including the C_{max}, area under the plasma concentration–time curve from zero to the last measurable sample time (AUC_{0-t}), and CL were analyzed by noncompartmental analysis using DAS software (version 3.1.6).

Ex Vivo DOX Fluorescence Imaging: Male Balb/C nude mice at 6 weeks of age were obtained from SLRC Laboratory Animal Company (Shanghai, China). All animals received care in compliance with the guidelines outlined in the Guide for the Care and Use of Laboratory Animals and all procedures were approved by the Animal Care and Use Committee of Jilin University. A human non-small-cell lung cancer xenograft tumor model was generated by subcutaneous injection of A549 cells (1.5×10^6) in the right flank of each mouse. When the tumor volumes reached 100–200 mm^3, the mice were administered intravenously with free DOX and CMC-ME_2MO-DOX at a DOX dose of 5 mg kg^{-1}. The mice were sacrificed 3, 10, and 24 h post-injection. The tumor and major organs (heart, liver, spleen, lung, and kidney) were excised, followed by washing the surface with physiological saline three times for ex vivo imaging of DOX fluorescence using the Maestro in vivo Imaging System (Cambridge Research & Instrumentation, Inc., USA). The resulting data can be used to identify, separate, and remove the contribution of autofluorescence in analyzed images by the commercial software (Maestro 2.4). The average signals were also quantitatively analyzed using Maestro 2.4 software.

Evaluation of Maximum Tolerated Dose: Male Kunming mice (at 5–6 weeks of age, provided by Laboratory Animal Center of Jilin University) were used to evaluate the MTD of free DOX, and CMC-ME_2MO-DOX. All groups ($n = 3$) received a single dose by intravenous injection. The control groups received PBS or 50, 100, 150, and 200 mg kg^{-1} of CMC–ME_2MO. Five groups of mice received free DOX or CMC-ME_2MO-DOX at a dose of 5, 10, 15, 20, and 25 mg kg^{-1} DOX. The body weight and physical states of all the mice were monitored for a period of 10 d. The MTD was defined as the allowance of a median body weight loss of 20% and causes neither death due to toxic effects nor remarkable changes in the general signs within 10 d after administration.[44]

In Vivo Antitumor Efficiency: A human non-small-cell lung cancer xenograft tumor model was generated by subcutaneous injection of A549 cells (1.5×10^6) in the right flank of each mouse as described above. When the tumor volume was approximately 50 mm^3, mice were randomly divided into six groups. Animals were treated with PBS, free DOX (3.0 mg kg^{-1}), endostar (8.0 mg kg^{-1}), free DOX (3.0 mg kg^{-1}) plus endostar (8.0 mg kg^{-1}), CMC-ME_2MO-DOX (3.0 mg kg^{-1} DOX eq.), and CMC-ME_2MO-DOX (3.0 mg kg^{-1} DOX eq.) plus endostar (8.0 mg kg^{-1}) by intravenous injection on days 0, 4, 8, and 12. In the combination treatment group, endostar was injected 1 h after the treatment of DOX or CMC-ME_2MO-DOX. The treatment efficacy and systemic toxicity were assessed by measuring the tumor volume and body weight, respectively. The tumor volume and tumor suppression rate were calculated by the following formula:

$$\text{Tumor volume } (V) = a \times b^2/2$$

$$\text{The tumor growth rate (TGR,\%)} = V_t / V_0 \times 100\%$$

$$\text{Tumor suppression rate (TSR,\%)} = [(TGR_c - TGR_x) / TGR_c)] \times 100\%$$

a and b are the longest and shortest diameter of the tumors measured by vernier caliper. V_0 represented the initial tumor volume at day 0. "c" represents the control group, while "x" represents the treatment group.

Histological and Immunohistochemical Analyses: The mice were sacrificed at day 18 and the tumors and major organs (heart, liver, spleen, lung, and kidney) were collected, fixed in 4% PBS buffered paraformaldehyde overnight, and then embedded in paraffin. The paraffin-embedded tumors were cut at 5 µm thickness, and stained with H&E to assess histological alterations by microscope (Nikon TE2000U). Immunohistochemistry was performed as described previously.[23a,45] Rabbit monoclonal primary antibody for cleaved PARP1 (Abcam, Cambridge, MA, USA), Rabbit polyclonal primary antibody for CD31 (Abcam, Cambridge, MA, USA), and PV-6000 two-step immunohistochemistry kit (polymer detection system for immunohistological staining; Zhongshan Goldbridge Biotechnology, Beijing, China) were used in this study.

In Situ Terminal Deoxynucleotidyl Transferase–Mediated Deoxyuridine Triphosphate Nick End Labeling (TUNEL) Assay: TUNEL assay was performed using a FragELTM DNA fragment detection kit (colorimetric-TdT Enzyme method) according to the manufacturer's protocol (EMD chemicals Inc, Darmstadt, Germany).

Statistical Analysis: All experiments were performed at least three times and expressed as means ± SD. Data were analyzed for statistical significance using Student's test. A value of $p < 0.05$ was considered statistically significant, and a value of $p < 0.01$ was considered highly significant.

Acknowledgements

This research was financially supported by National Natural Science Foundation of China (Projects 51173184, 51373168, 51390484, 51233004, and 51321062), Ministry of Science and Technology of China (International Cooperation and Communication Program 2011DFR51090) and Program of Scientific Development of Jilin Province (20130727050YY, 20130521011JH, and 20130206066GX).

Received: February 20, 2014
Revised: March 30, 2014
Published online:

[1] a) E. Van Cutsem, S. de Haas, Y. K. Kang, A. Ohtsu, N. C. Tebbutt, J. M. Xu, W. P. Yong, B. Langer, P. Delmar, S. J. Scherer, M. A. Shah, *J. Clin. Oncol.* **2012**, *30*, 2119; b) H. Wang, Y. Wu, R. F. Zhao, G. J. Nie, *Adv. Mater.* **2013**, *25*, 1616; c) Y. Zhou, J. Yang, J. S. Rhim, J. Kopecek, *J. Controlled Release* **2013**, *172*, 946; d) D. Zhou, H. Xiao, F. Meng, X. Li, Y. Li, X. Jing, Y. Huang, *Adv. Healthcare Mater.*

2013, *2*, 822; e) M. Khan, Z. Y. Ong, N. Wiradharma, A. B. E. Attia, Y. Y. Yang, *Adv. Healthcare Mater.* **2012**, *1*, 373.
[2] D. F. Zhang, E. M. E. Hedlund, S. Lim, F. Chen, Y. Zhang, B. C. Sun, Y. H. Cao, *Proc. Natl. Acad. Sci. U.S.A.* **2011**, *108*, 4117.
[3] a) P. Carmeliet, R. K. Jain, *Nat. Rev. Drug Discovery* **2011**, *10*, 417; b) L. Brannon-Peppas, J. O. Blanchette, *Adv. Drug Delivery Rev.* **2012**, *64*, 206.
[4] A. Llevot, D. Astruc, *Chem. Soc. Rev.* **2012**, *41*, 242.
[5] a) X. H. Fu, J. Li, Y. Zou, Y. R. Hong, Z. X. Fu, J. J. Huang, S. Z. Zhang, S. Zheng, *Cancer Lett.* **2011**, *312*, 109; b) G. C. Jayson, D. J. Hicklin, L. M. Ellis, *Nat. Rev. Clin. Oncol.* **2012**, *9*, 297.
[6] a) T. Liu, L. Ye, Y. Z. He, X. M. Chen, J. Peng, X. M. Zhang, H. Yi, F. Peng, A. M. Leng, *Exp. Mol. Pathol.* **2011**, *91*, 745; b) A. A. M. Van der Veldt, M. Lubberink, I. Bahce, M. Walraven, M. P. de Boer, H. Greuter, N. H. Hendrikse, J. Eriksson, A. D. Windhorst, P. E. Postmus, H. M. Verheul, E. H. Serne, A. A. Lammertsma, E. F. Smit, *Cancer Cell* **2012**, *21*, 82.
[7] S. Huang, K. Shao, Y. Liu, Y. Kuang, J. Li, S. An, Y. Guo, H. Ma, C. Jiang, *ACS Nano* **2013**, *7*, 2860.
[8] a) H. Xiao, W. Li, R. Qi, L. Yan, R. Wang, S. Liu, Y. Zheng, Z. Xie, Y. Huang, X. Jing, *J. Controlled Release* **2012**, *163*, 304; b) T. M. Allen, P. R. Cullis, *Science* **2004**, *303*, 1818; c) H. X. Chen, J. N. Cleck, *Nat. Rev. Clin. Oncol.* **2009**, *6*, 465; d) S. M. Lee, T. V. O'Halloran, S. T. Nguyen, *J. Am. Chem. Soc.* **2010**, *132*, 17130.
[9] R. Wang, S. K. Qin, Y. Q. Chen, Y. M. Li, C. J. Chen, Z. S. Wang, R. S. Zheng, Q. Wu, *Oncol. Rep.* **2012**, *28*, 439.
[10] M. J. Bissell, W. C. Hines, *Nat. Med.* **2011**, *17*, 320.
[11] X. Q. Li, B. Y. Shang, D. C. Wang, S. H. Zhang, S. Y. Wu, Y. S. Zhen, *Cancer Lett.* **2011**, *301*, 212.
[12] H. T. Ta, C. R. Dass, I. Larson, P. F. M. Choong, D. E. Dunstan, *Biomaterials* **2009**, *30*, 3605.
[13] a) M. J. Ernsting, W. L. Tang, N. W. MacCallum, S.-D. Li, *Biomaterials* **2012**, *33*, 1445; b) M. J. Ernsting, W.-L. Tang, N. MacCallum, S. D. Li, *Bioconjugate Chem.* **2011**, *22*, 2474; c) M. J. Ernsting, W. D. Foltz, E. Undzys, T. Tagami, S. D. Li, *Biomaterials* **2012**, *33*, 3931; d) H. Qian, X. Wang, K. Yuan, C. Xie, W. Wu, X. Jiang, L. Hu, *Biomater. Sci.* **2014**, *2*, 220.
[14] a) W. Wang, J. X. Ding, C. S. Xiao, Z. H. Tang, D. Li, J. Chen, X. L. Zhuang, X. S. Chen, *Biomacromolecules* **2011**, *12*, 2466; b) Z. Cao, S. Jiang, *Nano Today* **2012**, *7*, 404.
[15] a) A. T. Reza, S. B. Nicoll, *Acta Biomater.* **2010**, *6*, 179; b) P. S. Mallur, M. P. Morrison, G. N. Postma, M. R. Amin, C. A. Rosen, *Laryngoscope* **2012**, *122*, 322; c) N. A. Ramli, T. W. Wong, *Int. J. Pharm.* **2011**, *403*, 73; d) M. J. Ernsting, M. Murakami, E. Undzys, A. Aman, B. Press, S. D. Li, *J. Controlled Release* **2012**, *162*, 575.
[16] a) S. A. Bencherif, A. Srinivasan, F. Horkay, J. O. Hollinger, K. Matyjaszewski, N. R. Washburn, *Biomaterials* **2008**, *29*, 1739; b) T. T. Nielsen, V. Wintgens, C. Amiel, R. Wimmer, K. L. Larsen, *Biomacromolecules* **2010**, *11*, 1710; c) C. E. Schante, G. Zuber, C. Herlin, T. F. Vandamme, *Carbohydr. Polym.* **2011**, *85*, 469.
[17] a) C. Y. Long, M. M. Sheng, B. He, Y. Wu, G. Wang, Z. W. Gu, *Chin. J. Polym. Sci.* **2012**, *30*, 387; b) W. Xu, I. A. Siddiqui, M. Nihal, S. Pilla, K. Rosenthal, H. Mukhtar, S. Gong, *Biomaterials* **2013**, *34*, 5244.
[18] X. Xu, Y. Li, H. Li, R. Liu, M. Sheng, B. He, Z. Gu, *Small* **2014**, *10*, 1133.
[19] a) M. Q. Li, Z. H. Tang, H. Sun, J. X. Ding, W. T. Song, X. S. Chen, *Polym. Chem.* **2013**, *4*, 1199; b) B. N. Khlebtsov, N. G. Khlebtsov, *Colloid J.* **2011**, *73*, 118.
[20] a) S. Dufort, L. Sancey, J.-L. Coll, *Adv. Drug Delivery Rev.* **2012**, *64*, 179; b) Y. Li, G. H. Gao, D. S. Lee, *Adv. Healthcare Mater.* **2013**, *2*, 388.
[21] W.-C. Huang, W.-H. Chiang, Y.-F. Huang, S.-C. Lin, Z.-F. Shih, C.-S. Chern, C.-S. Chiang, H.-C. Chiu, *J. Drug Targeting* **2011**, *19*, 944.
[22] C. Sanson, C. Schatz, J. F. Le Meins, A. Soum, J. Thevenot, E. Garanger, S. Lecommandoux, *J. Controlled Release* **2010**, *147*, 428.
[23] a) J. Dai, S. Lin, D. Cheng, S. Zou, X. Shuai, *Angew. Chem. Int. Ed.* **2011**, *50*, 9404; b) Y. Wu, S. Ihme, M. Feuring-Buske, S. L. Kuan, K. Eisele, M. Lamla, Y. Wang, C. Buske, T. Weil, *Adv. Healthcare Mater.* **2013**, *2*, 884.
[24] X. Yang, J. J. Grailer, I. J. Rowland, A. Javadi, S. A. Hurley, D. A. Steeber, S. Gong, *Biomaterials* **2010**, *31*, 9065.
[25] a) Y. S. Lai, Y. Lei, X. H. Xu, Y. L. Li, B. He, Z. W. Gu, *J. Mater. Chem. B* **2013**, *1*, 4289; b) N. J. Song, M. M. Ding, Z. C. Pan, J. H. Li, L. J. Zhou, H. Tan, Q. Fu, *Biomacromolecules* **2013**, *14*, 4407.
[26] a) R. Wei, L. Cheng, M. Zheng, R. Cheng, F. Meng, C. Deng, Z. Zhong, *Biomacromolecules* **2012**, *13*, 2429; b) D. M. Ren, M. Dalmau, A. Randall, M. M. Shindel, P. Baldi, S. W. Wang, *Adv. Funct. Mater.* **2012**, *22*, 3170.
[27] a) Y. Sun, W. Zou, S. Bian, Y. Huang, Y. Tan, J. Liang, Y. Fan, X. Zhang, *Biomaterials* **2013**, *34*, 6818; b) S. M. Lee, H. J. Kim, Y. J. Ha, Y. N. Park, S. K. Lee, Y. B. Park, K. H. Yoo, *ACS Nano* **2013**, *7*, 50.
[28] S. D. Li, S. B. Howell, *Mol. Pharm.* **2010**, *7*, 280.
[29] M. ***Šťastný, D. Plocová, T. Etrych, K. Ulbrich, B. Říhová, *Eur. J. Cancer* **2002**, *38*, 602.
[30] P. A. Ma, S. Liu, Y. B. Huang, X. S. Chen, L. P. Zhang, X. B. Jing, *Biomaterials* **2010**, *31*, 2646.
[31] X. Wang, X. Zhen, J. Wang, J. Zhang, W. Wu, X. Jiang, *Biomaterials* **2013**, *34*, 4667.
[32] A. L. Lee, S. Venkataraman, S. B. Sirat, S. Gao, J. L. Hedrick, Y. Y. Yang, *Biomaterials* **2012**, *33*, 1921.
[33] S. Y. Lee, S. Kim, J. Y. Tyler, K. Park, J. X. Cheng, *Biomaterials* **2013**, *34*, 552.
[34] X. C. Peng, M. Qiu, M. Wei, B. X. Tan, J. Ge, Y. Zhao, Y. Chen, K. Cheng, Y. Zhou, Y. Wu, F. M. Gong, Q. Li, F. Xu, F. Bi, J. Y. Liu, *Cancer Chemother. Pharmacol.* **2012**, *69*, 239.
[35] Y. Li, X. E. Huang, P. W. Yan, Y. Jiang, J. Xiang, *Asian Pac. J. Cancer Prev.* **2010**, *11*, 1119.
[36] S. Yu, J. Ding, C. He, Y. Cao, W. Xu, X. Chen, *Adv. Healthcare Mater.* **2014**, *3*, 752.
[37] H. Zhang, J. Wang, W. Mao, J. Huang, X. Wu, Y. Shen, M. Sui, *J. Controlled Release* **2013**, *166*, 147.
[38] a) C. Fu, L. Lin, H. Shi, D. Zheng, W. Wang, S. Gao, Y. Zhao, H. Tian, X. Zhu, X. Chen, *Biomaterials* **2012**, *33*, 4589; b) L. Virág, A. Robaszkiewicz, J. M. Rodriguez-Vargas, F. J. Oliver, *Mol. Aspects Med.* **2013**, *34*, 1153.
[39] a) Y. Amoh, L. N. Li, M. Yang, P. Jiang, A. R. Moossa, K. Katsuoka, R. M. Hoffman, *Cancer Res.* **2005**, *65*, 2337; b) Y. Yang, D. Pan, K. Luo, L. Li, Z. Gu, *Biomaterials* **2013**, *34*, 8430.
[40] a) C. Aderhold, C. Umbreit, A. Faber, A. Sauter, J. U. Sommer, R. Birk, P. Erben, R. D. Hofheinz, J. Stern-Straeter, K. Hormann, J. D. Schultz, *Anticancer Res.* **2013**, *33*, 1951; b) J. Yamao, H. Toyokawa, S. Kim, S. Yamaki, S. Satoi, H. Yanagimoto, T. Yamamoto, S. Hirooka, Y. Matsui, A. H. Kwon, *J. Hepatobiliary Pancreat. Sci.* **2013**, *20*, 206.
[41] a) J. Shilpa, M. A. Pretty, M. Anitha, C. S. Paulose, *Eur. J. Pharmacol.* **2013**, *715*, 154; b) I. R. Corbin, R. Buist, V. Volotovskyy, J. Peeling, M. Zhang, G. Y. Minuk, *Hepatology* **2002**, *36*, 345.
[42] M. Li, W. Song, Z. Tang, S. Lv, L. Lin, H. Sun, Q. Li, Y. Yang, H. Hong, X. Chen, *ACS Appl. Mater. Interfaces* **2013**, *5*, 1781.
[43] a) H.-J. Cho, I.-S. Yoon, H. Y. Yoon, H. Koo, Y.-J. Jin, S.-H. Ko, J.-S. Shim, K. Kim, I. C. Kwon, D.-D. Kim, *Biomaterials* **2012**, *33*, 1190; b) S. Zhu, M. Hong, G. Tang, L. Qian, J. Lin, Y. Jiang, Y. Pei, *Biomaterials* **2010**, *31*, 1360.
[44] J. Kato, Y. Li, K. Xiao, J. S. Lee, J. Luo, J. M. Tuscano, R. T. O'Donnell, K. S. Lam, *Mol. Pharm.* **2012**, *9*, 1727.
[45] M. Li, S. Lv, Z. Tang, W. Song, H. Yu, H. Sun, H. Liu, X. Chen, *Macromol. Biosci.* **2013**, *13*, 1150.